Deciphering the Dynamics of Interlocked Feedback Loops in a Model of the Mammalian Circadian Clock

D. Battogtokh and **J. J. Tyson**

Abstract

Mathematical models of fundamental biological processes play an important role in consolidating theory and experiments, especially if they are systematically developed, thoroughly characterized, and well tested by experimental data. In this work, we report a detailed bifurcation analysis of a mathematical model of the mammalian circadian clock network developed by Relogio et al. [16], noteworthy for its consistency with available data. Using one- and two-parameter bifurcation diagrams, we explore how oscillations in the model depend on the expression levels of its constituent genes and the activities of their encoded proteins. These bifurcation diagrams allow us to decipher the dynamics of interlocked feedback loops, by parametric variation of genes and proteins in the model. Among other results, we find that REV-ERB, a member of a subfamily of orphan nuclear receptors, plays a critical role in the intertwined dynamics of Relogio's model. The bifurcation diagrams reported here can be used for predicting how the core-clock network responds - in terms of period, amplitude and phases of oscillations - to different perturbations.

Keywords: circadian rhythm, network dynamics, bifurcation analysis

Introduction

In the last two decades, there has been tremendous progress in understanding how circadian oscillations are generated and how rhythmicity is sustained in the cells and tissues of many species of animals, plants and fungi [1-7]. It has been established that in all these organisms, core clock genes constitute a 'circadian network' that generates endogenous oscillations by repression of the transcription of these clock genes by their own proteins, i.e., by delayed negative-feedback in the transcription-translation-repression loop. Mathematically, these robust rhythms arise as limit cycle oscillations at Hopf bifurcation points [8-10]. Different research groups have implemented this general mechanism in their own unique models of circadian clocks [11-14].

In systems biology, mathematical models are of special utility if they explain a vast amount of experimental data and can be investigated by analytic tools [15]. Recently, Relogio et al developed a mathematical model of the mammalian circadian-clock network [16], expressed as a set of 20 ordinary differential equations (ODE's), including 76 kinetic parameters. Simulations of Relogio's model are in good agreement with known experimental data [16].

The mammalian circadian-clock network drives ~24 h rhythms in the activity of a heterodimeric transcription factor, CLOCK/BMAL, which drives the expression of other clock genes, including *PERIOD* (*PER*), *CRYPTOCHROME* (*CRY*), *REV-ERB*α and β (*REV*), and *RORa, b* and *c* (*ROR*). PER/CRY heterodimers bind to and inhibit CLOCK/BMAL, whereas ROR acts as an activator and REV acts as a repressor of CLOCK/BMAL-driven transcription. Different models of the mammalian circadian clock join together these feedback loops in different ways. Some models view the PER/CRY loop as the master oscillator, with the REV and ROR loops providing fine-tuning and robustness to the oscillations [11-13, 17, 18]. In Relogio's model, on the other hand, the feedback loops are not hierarchical, but rather they orchestrate the rhythm synergistically. Understanding the dynamics of interlocked negative and positive feedback loops, such as the loops

present in the mammalian circadian-clock network, is an important and challenging problem [13, 14, 19, 20]. In this work, using bifurcation analysis [21], we decipher the dynamics of interlocked feedback loops in Relogio's model.

Despite all we know about the genes underlying the mammalian circadian clock, the molecular network is still not completely understood [22]. Future experiments may unveil yet unknown or underappreciated players critical for circadian rhythms in single cells and different tissues. Bifurcation analysis of network diagrams will be helpful for inferring the roles of possible new elements. Because many practical applications, especially analyses of clinical data, require extended mathematical models combining multiple networks in the cell [23-26], we suggest that bifurcation analysis will be useful for assessing the dynamics of the circadian clock network in integrated models of the broader physiology of mammalian cells [27, 28]. In addition, our characterization of the parameter space of a comprehensive model of the circadian clock network may be valuable resource for determining optimal rhythmic signals for the daily synchronization of a variety of cellular processes, especially synchronization of the cell division cycle by the circadian rhythm [24, 29, 30].

Methods

Relogio et al Model of the Mammalian Circadian Clock Network

In Figure 1 we show the wiring diagram of the circadian clock network proposed by Relogio et al for the murine circadian clock in a single cell [16]. The central node of the network is a heterodimeric transcription factor, CLOCK/BMAL, the yellow box in the center of Figure 1. The core clock genes, *PER, CRY, Bmal, REV*, and *ROR*, are represented by blue oval boxes in the nucleus. Clock proteins in the cytoplasm are shown as purple boxes. PER and CRY proteins form multimeric complexes and enter into the nucleus, where they interact with CLOCK/BMAL. The PER/CRY complex represses CLOCK/BMAL-activated transcriptions, thereby creating a delayed negative-feedback loop in the transcription-translation process. We will refer to this delayed negative-feedback loop as the 'PC loop', and we will refer to the PER/CRY heterodimeric complex hereafter as the 'PC complex'. The PC complex is degraded at night, releasing its inhibitory effect on CLOCK/BMAL, to allow a fresh restart of the transcription of clock genes [16].

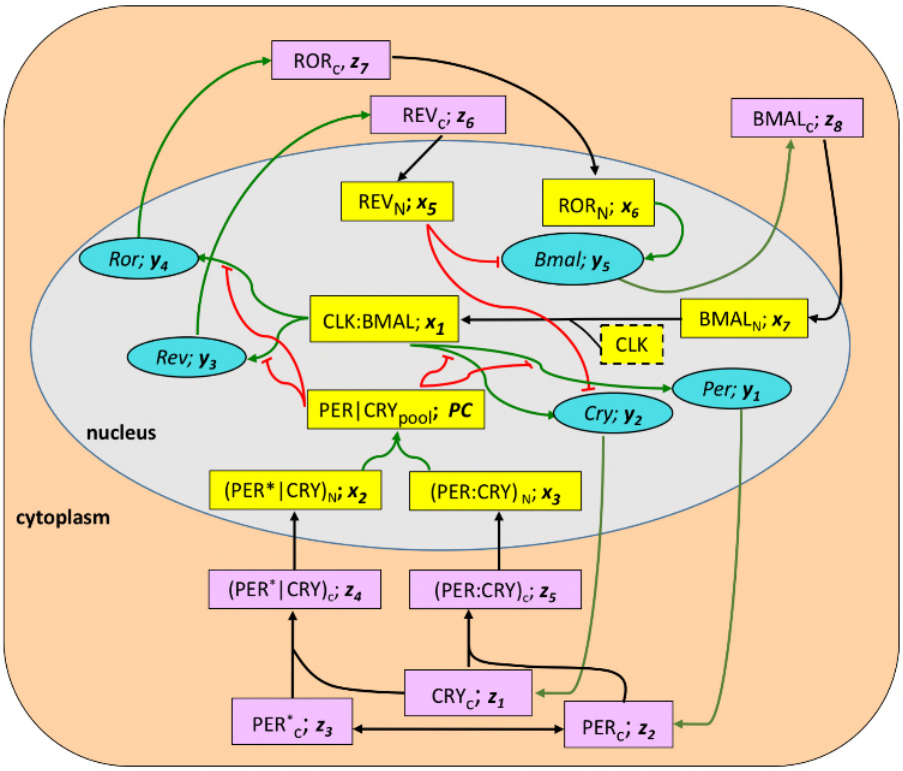

Figure 1. Wiring diagram of Relogio's model of the circadian clock network in mammalian cells. Core circadian-clock mRNAs and proteins are indicated by ovals and rectangles, respectively. Within each oval and rectangle is the name of the component followed by the name of its variable in Relogio's model (Eqs. S1-S19 in Suppl. Text S1). Black arrows indicate transport steps (cytoplasm to nucleus) or chemical reactions (e.g., phosphorylation, indicated by an asterisk*, or association of two proteins to form a complex). Green arrows indicate "activation" of one component by another (e.g., the CLK:BMAL transcription factor activates synthesis of *Per* mRNA in the nucleus, which in turn activates synthesis of PER protein in the cytoplasm). Red lines, with blunt tips, indicate "inhibition" effects (e.g., nuclear REV inhibits the transcription of *Bmal* and *Cry* mRNAs). In Relogio's model, CLK protein is assumed to be present in constant excess, so there is no time-dependent variable for this protein.

ROR and REV proteins in the nucleus can bind to the promoter region of the *BMAL* gene and modulate the expression of *Bmal* mRNA. In doing so, ROR acts as an activator, and REV acts as a repressor. Following Relogio et al. [16], we will refer to these feedback effects as the 'RBR loop'. An important feature of Relogio's model is that the RBR loop can generate and maintain oscillations autonomously. When the PC loop is maintained constitutively active (non-oscillatory), sustained oscillations continue to be generated by RBR loop (see the simulations in Fig. 3B of Ref. [16]). Furthermore, when *REV* (or *ROR*) is overexpressed, circadian rhythmicity can be lost (see the simulations in Fig. 3C and Fig. 6A-B of Ref. [16]) [16, 31]. These in *silico* predictions of the

model were confirmed by *RORa* and *REV-ERBα* overexpression in a human osteosarcoma cell line, U2OS (see Fig. 7 of Ref. [16]).

Notice that the RBR loop is actually the union of two loops: a REV loop (a negative-feedback transcription-translation loop) and a ROR loop (a union of two positive and a negative feedback transcription-translation loops). We shall make this distinction later.

Numerical methods

The differential equations of Relogio's model are provided in Suppl. Text S1. The variables of the model are listed in Suppl. Table S1, and WT (wild type) parameter values are provided in Suppl. Table S2. Numerical simulations of the model were carried out in Mathematica [32] and bifurcation diagrams were calculated using AUTO [33].

Bifurcation diagrams

We use one- and two-parameter bifurcation diagrams to characterize the dependence of solutions of Relogio's differential equations (S1-S19 in Suppl. Text S1) on the values of certain kinetic parameters in the model equations. In a one-parameter bifurcation diagram, the chosen kinetic parameter is plotted as the independent variable (the horizontal axis) and some indicator of the output of the model is plotted as the dependent variable (the vertical axis). Typically, the magnitude of a dynamic variable in the model is chosen as the dependent variable, in which cases the one-parameter bifurcation diagram shows the asymptotic behavior of this molecular component as a function of changes in the chosen kinetic parameter. In particular, the diagram shows how the steady-state value of the dynamic variable changes with the bifurcation parameter and how the amplitude of any periodic solutions, bifurcating from the steady state, changes with the bifurcation parameter. The diagram also indicates whether the steady states and periodic solutions are asymptotically stable or unstable.

We also use one-parameter bifurcation diagrams to indicate how the period of oscillatory solutions depends on a parameter value and how the phases of oscillatory components change, relative to one another, as the parameter value changes. In this way, we can use one-parameter bifurcation diagrams to succinctly summarize how the amplitude, period and phase of oscillations depend on the values of the kinetic parameters in a dynamical model of circadian rhythms.

We use two-parameter bifurcation diagrams to characterize the domain of oscillations on the plane of two chosen bifurcation parameters. We calculate period distributions inside the oscillatory domains and mark the regions of different periods with different symbols.

Results

One-Parameter Bifurcation Diagrams

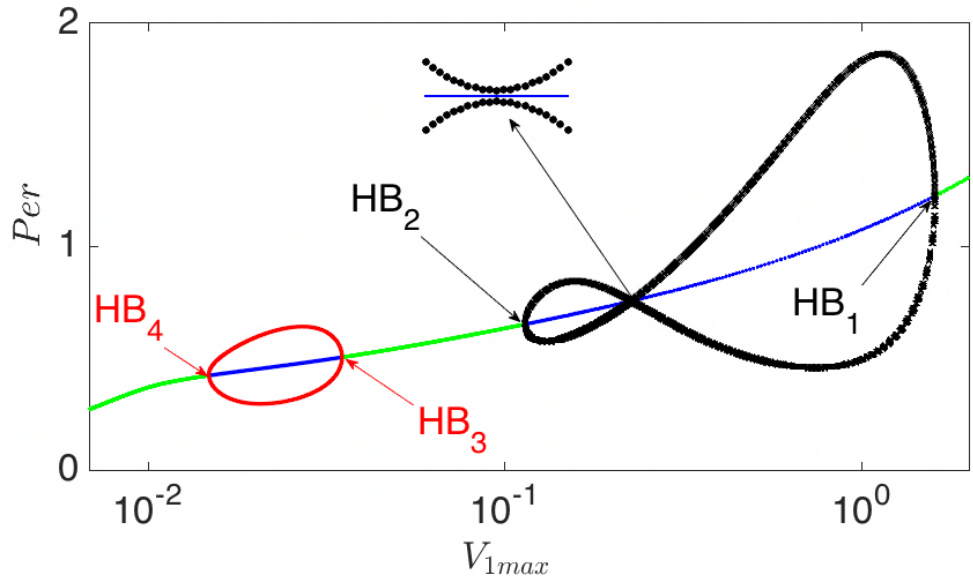

Figure 2. A one-parameter bifurcation diagram of Relogio's model. The transcription rate of the *PER* gene, V_{1max}, is used as the primary bifurcation parameter. Green lines: stable steady states; blue lines: unstable steady states. There are four Hopf bifurcation points in this diagram, HB_i, $i = 1..4$. The black and red curves show maximum and minimum amplitudes of the oscillations.

Modulations of PER expression. The one-parameter bifurcation diagram in Figure 2 shows how the amplitude of periodic solutions depends on the transcription rate of *Per* mRNA, V_{1max}. All other parameters are fixed at WT values (Supplementary Table II). In the interval $V_{1max} \in [0.142, 1.63]$, the model displays stable limit cycle oscillations with a circadian period. Notice that, at $V_{1max} \approx 0.25$, there is a significant decrease of *Per* mRNA amplitude, due to multiple repressions exerted on the transcription of the *PER* gene. As reported in Ref. [16], there are small amplitude oscillations of long period ($T \approx 50$ h) at small values of V_{1max}. The two oscillatory domains in Figure 2 are separated by stable steady-state solutions.

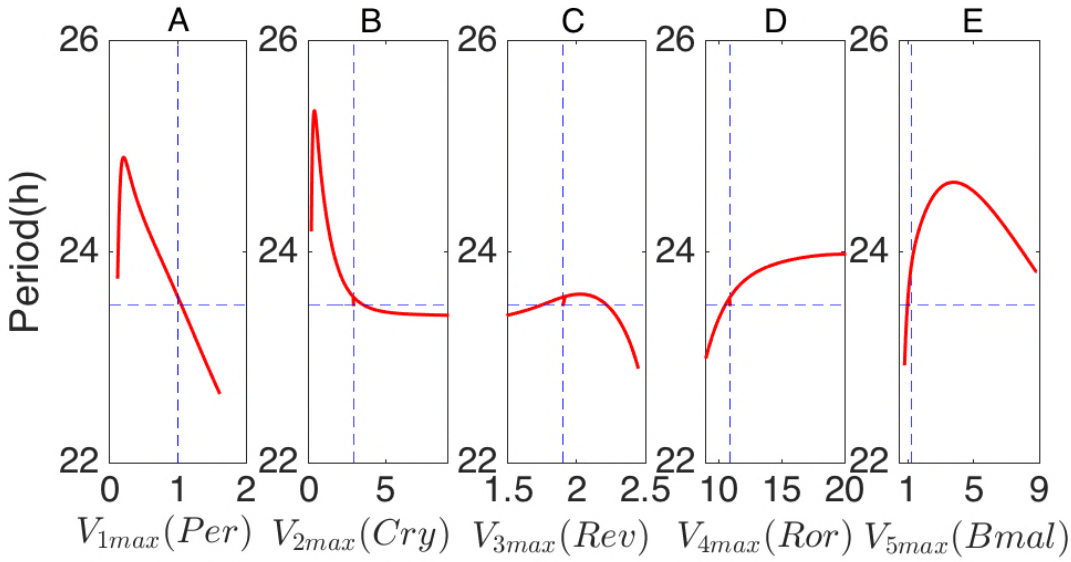

Figure 3. Oscillation period vs $V_{imax}, i = 1..5$, the transcription rates of *Per*, *Cry*, *Rev*, *Ror*, and *Bmal* mRNAs. The periods of oscillation are plotted between the Hopf bifurcation points HB_1 and HB_2 in Figure 2. Vertical dashed lines mark the value of the bifurcation parameter corresponding to WT rhythm (period = 23.5 h)

The period vs transcription rates. Rhythmic dynamics in a circadian network can be characterized by the period, amplitude, and phase of oscillations. The period is common to all variables, while the amplitudes and phases vary from one component to another. The red curves in Figure 3 show that the oscillation period changes non-monotonically with changing transcription rates of the core clock genes, $V_{imax}, i = 1..5$. An interesting feature in Figure 3 is that except for *Ror*, the period decreases with the increase of transcription rates from WT values, indicating that the network reacts to *Ror's* increase differently compared to increases of other mRNAs.

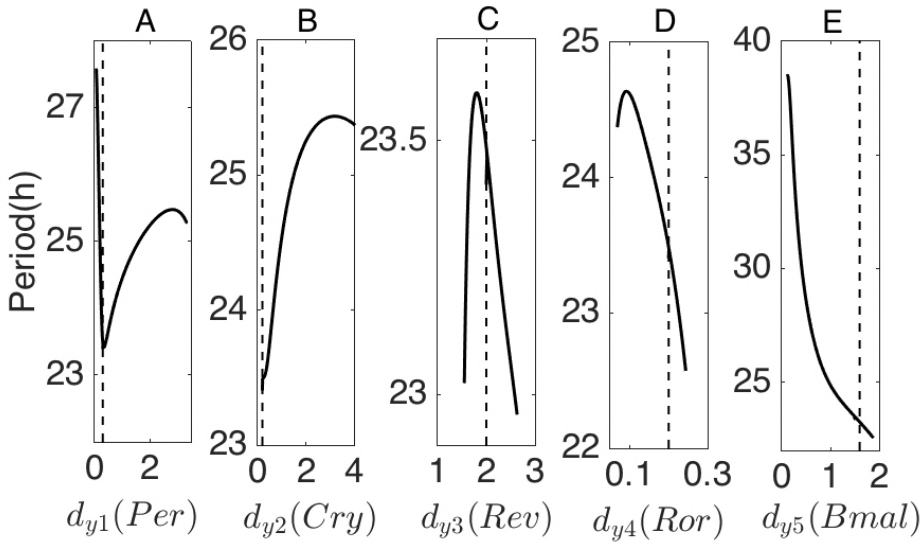

Figure 4. Period vs degradation rates, $d_{yi}, i = 1..5$, of *Per*, *Cry*, *Rev*, *Ror*, and *Bmal* mRNAs. Black dashed lines mark WT values of the bifurcation parameters.

Period vs degradation rates. Figure 4 shows how the period of oscillation changes with modulations of mRNA degradation rates. Period increases as the degradation rates of *Per* and *Cry* mRNAs increase above their WT values and decreases as the degradation rates of mRNAs in the RBR loop increase above their WT values. In the case of *Rev*, the period change is limited to a narrow interval [23 h, 23.7 h], whereas the period change is much more pronounced for variations in the degradation rates of *Ror* and *Bmal*. An interesting feature for *Bmal* is that the period is no longer "circadian" for small values of d_{y5}.

Phase relations vs transcription rates. We define the phase of oscillations as the time when mRNA level of a core clock gene reaches its maximum level, relative to the phase of a reference mRNA. Figure 5 shows that phases do not change significantly with modulations of transcription rates. In general, the phase of *Cry* is most sensitive to changes of the transcription rates. The phase of *Bmal* changes moderately with changes of transcription rates of the RBR loop. With changing rate of transcription of the *PER* gene, the phases of *Ror* and *Bmal* are locked, but the phases of *Rev* and *Cry* change slightly. With changing rate of transcription of the *REV* gene, the phase of *Ror* is locked, but the phases of *Bmal, Rev* and *Cry* change slightly.

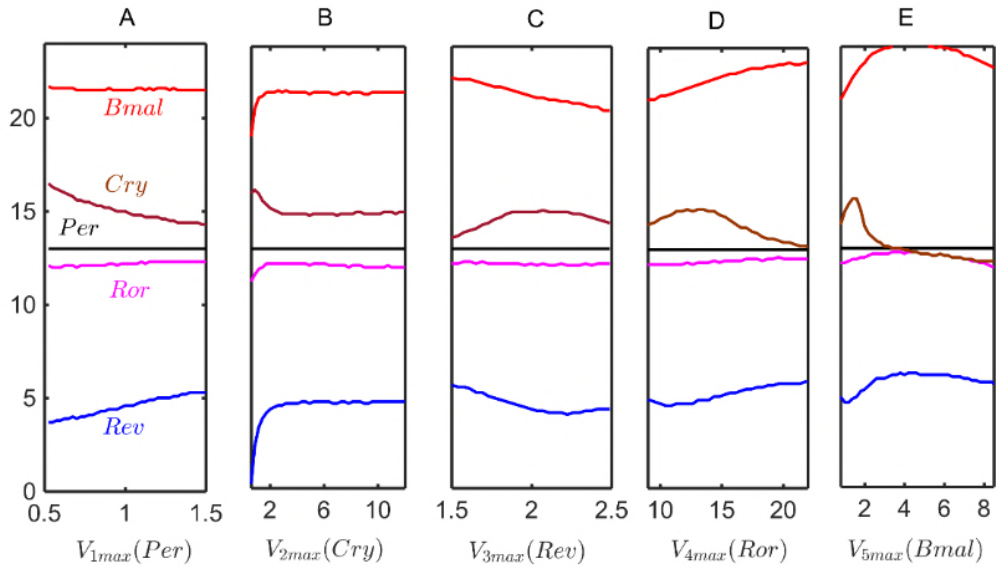

Figure 5. Phases of oscillations vs $V_{imax}, i = 1..5$, the transcription rates of *Per*, *Cry*, *Rev*, *Ror*, and *Bmal* mRNAs. Other parameters are fixed at WT values. In these plots, "phase" is the time of maximum expression of the mRNA, relative to the maximum expression of *Per*, which is fixed at 13 h.

Amplitudes vs transcription rates. Figure 6 shows the changes of the difference between maximum and minimum of amplitudes $(A_{max} - A_{min})$ of oscillations with the change of transcription rates. The amplitude of *Per* does not change significantly in Figure 6, indicating robustness of *Per* amplitude. The amplitude of *Ror* also does not change significantly. On the contrary, the amplitude of *Rev* is most sensitive to the modulations of transcription rates. The amplitude of *Cry* is sensitive to $V_{2max}(Cry)$, as well as to the modulations of positive feedbacks via $V_{4max}(Ror)$ and $V_{5max}(Bmal)$. The amplitude of *Bmal* decreases at large values of transcription rates.

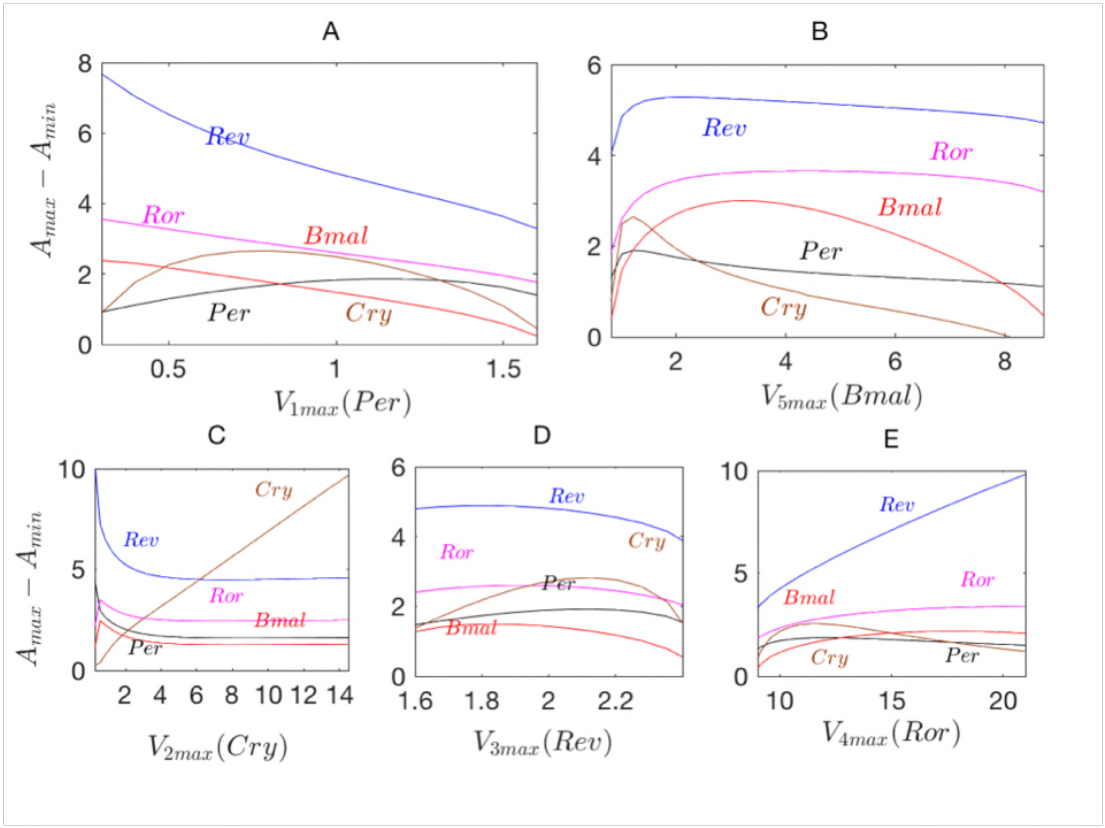

Figure 6. Dependence of the amplitude of oscillations (the difference between the maximum and minimum of oscillations) on the transcription rates $V_{imax}, i = 1..5$. Other parameters are fixed at WT values.

Interactions between the circadian clock and RAS/MAPK signaling networks. The dynamics of period, amplitude, and phases, obtained by bifurcation analysis can be used for practical purposes. Experimental data about the interactions between RAS/MAPK and the core clock network can be simulated using Relogio model. The RAS/MAPK signaling pathway may disrupt normal functioning of the core clock network by modulating the circadian period [34, 35]. It is known that changes in *RAS* expression alter directly the dynamics of *BMAL* [34]. Therefore, perturbation of the core clock network by RAS signaling has been studied by introducing a parameter k_{tt}, which modulates the strength of the transcription factor CLK:BMAL (variable x_1) for the expression of every clock gene [34, 35]. We refer to the S1 text of Ref. [35] for the definition of k_{tt}. In Figure 7 we show how period, *Per*'s amplitude, and the phases of oscillation change with k_{tt}. The WT value of $k_{tt} = 1$.

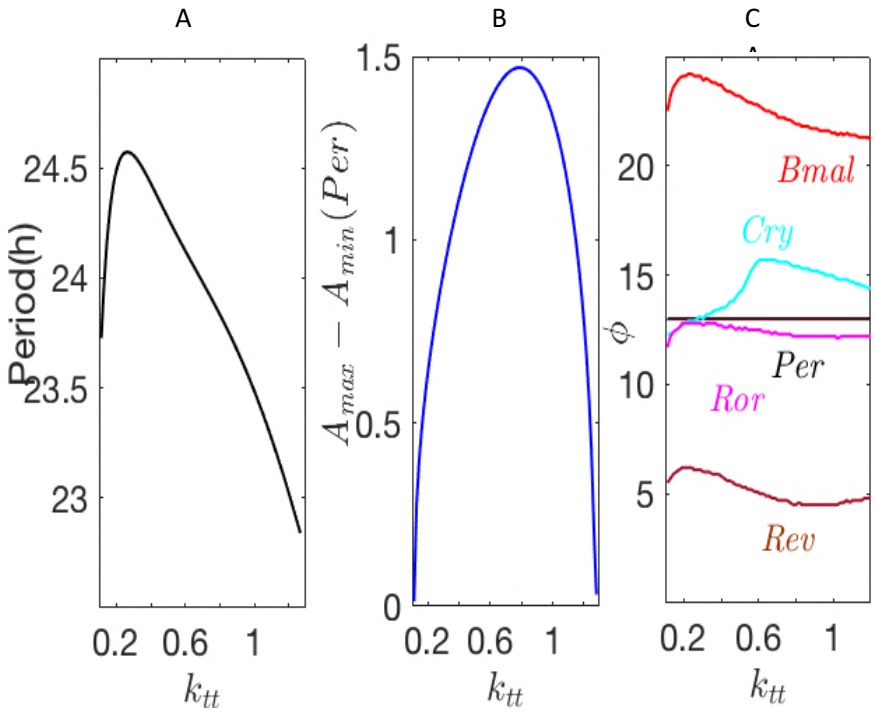

Figure 7. The effects of RAS signaling on the circadian clock network. Parameter k_{tt} modulates the strength of transcriptional factor CLK:BMAL. A) Period. B) Maximum amplitude of *Per* oscillations. C) Phases of oscillation (relative to the phase of *Per2* (black line) which is fixed at 13 h).

Notice qualitative similarities between the periods in Figure 3A and Figure 7A, as well as between *Per*'s amplitude in Figure 6A and Figure 7B. Recall that Figure 3A and Figure 6A show the network's response to the modulation of *Per*'s transcription rate, whereas Figure 7A-B show the RAS/MAPK pathway's interference on *Bmal*'s transcriptional activation. The period change in Figure 7A is similar to the period change in Figure 3A where V_{1max}(transcription rate of *Per*) is modulated, suggesting that *Bmal* activates strongly *Per*'s transcription. Interestingly, the changes of oscillation phases with k_{tt} are similar to phase changes in Figure 5E, where V_{5max} (the transcription rate of *Bmal*) is modulated.

Figure 7 suggests that by monitoring the changes in the expression patterns of a given clock gene caused by modulations from other pathways in the cell, qualitative changes in the period, amplitudes, and phases of oscillations can be inferred from bifurcation diagrams in Figure 3-6. As an example, an antisense transcript, *Per2AS*, of the *PER2* gene may depress the transcription rate of its sense counterpart, *Per2* [34]. Figure 6A shows how the level of *Per2* will be reduced when V_{1max} is depressed. Furthermore, according to Figure 3A, the period of oscillation is expected to increase, but according to Figure 5A, the phases of oscillations are expected to change slowly.

Detailed simulations of a mathematical model describing molecular interactions between sense and antisense transcripts are in agreement with these assessments [32] .

It was reported that the effects of RAS modulations on the core clock network can be described qualitatively by modulations of a single parameter, k_{t2} [34]. Suppl. Fig. S1 shows the changes of period, amplitude (*Per*), and phases of oscillations with the change of k_{t2} (Eq. (S12)). The main difference between modulations by k_{tt} and k_{t2} is in changes of *Cry* phase.

Two-Parameter Bifurcation Diagrams

Interactions between Bmal and Per. Figure 8 shows a two-parameter bifurcation diagram of Relogio's model for V_{1max} (*Per*) and V_{5max} (*Bmal*), transcription rates of a repressor and activator, respectively. The solid lines in Figure 8 are the loci of the four Hopf bifurcation points in Figure 2. Stable oscillations are found inside the solid curves. We marked the large oscillatory domain in Figure 8 with symbols of different colors to show the oscillation periods in different regions. In the simulations, we fixed all other parameters at WT values. Inside the small ellipse shown in Figure 8, we found the small-amplitude, long-period oscillations shown in Figure 2 by red symbols. The horizontal dashed line in Figure 8 shows that with the increase of V_{1max}, the domain of oscillations is replaced by stable, steady state solutions at $V_{1max} \approx 1.63$. We note that the oscillations outside the black lines are slowly damping oscillations.

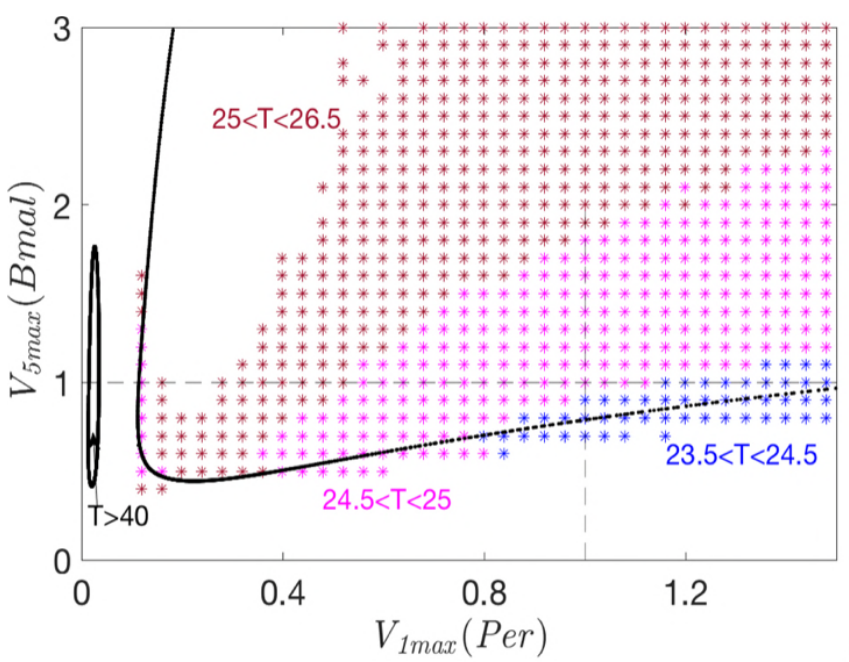

Figure 8. A two-parameter bifurcation diagram on the $(V_{1max}, V_{5\max})$ parameter plane. The symbols indicate the period of oscillations at a given location on the parameter plane. Dashed lines mark the WT values of V_{1max} and V_{5max}. Slow oscillations inside the small ellipse near $V_{1max} \approx 0.05$ correspond to the oscillations shown in Figure 2 by red symbols. In the white area inside the large domain, the period is greater than 26.5 h.

Period locking in the PC loop. Figure 9A shows a two-parameter bifurcation diagram on the parameter plane (V_{1max}, V_{2max}), the transcription rates of *Per* and *Cry*. The solid red curves in Figure 9A show the loci of Hopf bifurcation points HB_1 and HB_2 in Figure 2. Symbols of different colors mark the periods of oscillations. An interesting feature of Relogio's model is that the period of oscillation can be locked within a narrow interval, if either V_{1max} or V_{2max} is modulated alone. This can be seen, for example, by following the vertical dashed line in Figure 9, above the horizontal dashed line. In the case of V_{1max}'s modulation, V_{2max} must be set to a lower value than its WT value, in order to observe period-locking over a wide range of V_{1max} values.

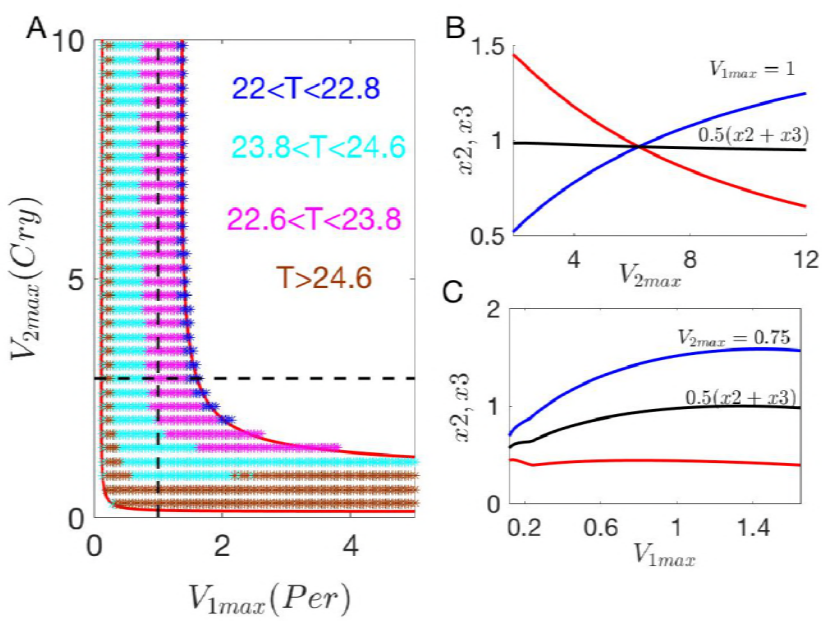

Figure 9. The dynamics of the PC loop. (A) Two-parameter bifurcation diagram on (V_{1max}, V_{2max}), all other parameters are fixed at their WT values. Symbols mark the period of oscillation. When $V_{1max} = 1$ (WT value), the period of oscillations is insensitive to changes of $V_{2max} > V_{2max}^{WT}$. Also, when $V_{2max} \leq 0.75$, the period is insensitive to the changes of V_{1max}. Dashed lines mark WT values of V_{1max} and V_{2max}. (B, C) The maximum amplitudes of $x2$(blue), $x3$(red), and PC (black) vs V_{2max}, when V_{1max} is fixed at 1, and vs V_{1max}, when V_{2max} is fixed at 0.75.

Figures 9B-C provide insight into period-locking in Relogio's model. These panels show how the maximum amplitudes of $x2$ (nuclear phosphorylated Per/Cry complex), $x3$ (nuclear unphosphorylated Per/Cry complex) and $PC = x2 + x3$ (PC pool) change with changes of V_{1max} and V_{2max}. With respect to increasing values of V_{2max} (panel B), $x2$ level increases (blue lines) and $x3$ level decreases (red lines), so that PC level is compensated (black lines). Consequently, the repression of core-clock genes by PC changes little with increasing V_{2max}. Thus, slow changes of PC restrain the period within a narrow interval. Figure 9C shows a similar compensation of PC, when V_{1max} is modulated, for $V_{2max} = 0.75$.

Interactions between PC *and* REV *loops.* In Figure 10 we explore the interplay of the negative-feedback transcription-translation loops, PC and REV. To this end, we introduce a new parameter α_{PC}, $PC = \alpha_{PC}(x2 + x3)$, to modulate the activity of PER/CRY in the nucleus: α_{PC} is used to boost PC activity up or turn down relative to the WT value, $\alpha_{PC} = 1$. The blue curve in Figure 10A shows the locus of HB_1 points (see Figure 2) on the ($V_{3max,}, \alpha_{PC}$) parameter plane. The periods of oscillations for V_{1max}^{WT} in different regions are marked by different symbols. Note that some of the symbols are outside of the blue lines because of $V_{1max}^{WT} \neq V_{1max}^{HB_1}$. All other parameters are fixed at WT values. Interestingly, the black symbols obtained by simulations reveal that there is another domain of oscillations on ($V_{3max,}, \alpha_{PC}$), where the period is $T > 32$ h. Because nuclear protein REV_N directly represses *Cry*, the PC loop is down regulated with the increase of V_{3max}. As a result, REV_N releases PC's repression of *Bmal,* allowing the REV loop, in cooperation with ROR and BMAL loops, to generate slow oscillations shown in Figure 10A.

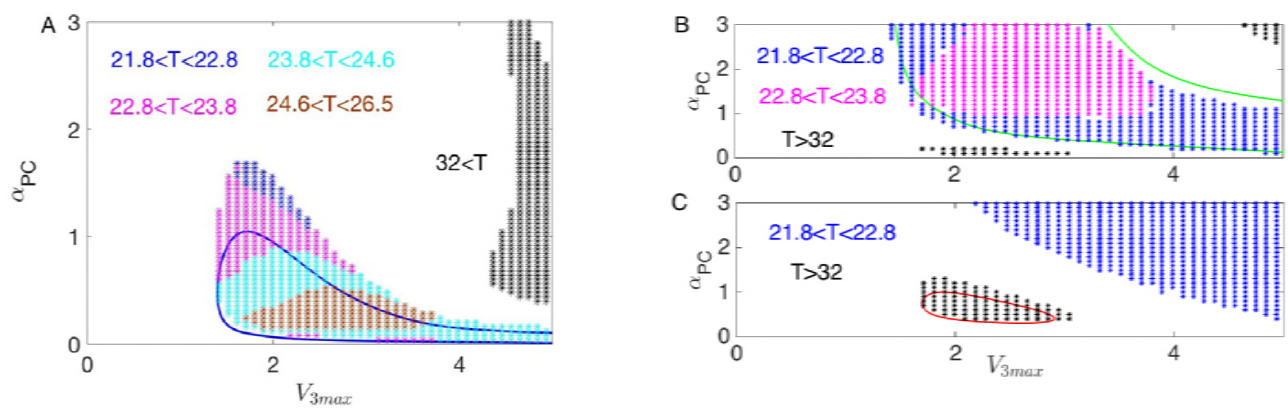

Figure 10. Interactions between the PC and REV loops, as revealed by two-parameter bifurcation diagrams. (A) The blue line shows the continuation locus of HB_1 in Figure 2. The symbols of different colors denote the oscillatory periods in different regions. Black symbols at $V_{3max} > 4$ show a domain of slow oscillations. (B) Green lines show the continuation of HB_2 in Figure 2. (C) Red curve shows the continuation of HB_3 in Figure 2.

In Figure 10B we show the continuation of the bifurcation point HB_2 in Figure 2. Blue and purple symbols mark oscillation periods at $V_{1max} = V_{1max}^{HB2}$. Because $V_{1max}^{HB2} < V_{1max}^{WT}$, the amplitude of *Per* oscillations is low. Black symbols in Figure 10B show that besides the oscillatory domain inside the loci of HB_2, there are two separate domains of slow oscillations on (V_{3max}, α_{PC}). As the

lower domain of slow oscillations persist at $\alpha_{PC} \approx 0$, here the strength of PC loop is negligible compared to REV's repression. As for the upper slow domain, though α_{PC} is strong in this region, V_{3max} is even stronger; hence, the RBR loop can independently generate slow oscillations.

The red curve in Figure 10C shows the continuation of the bifurcation point HB_3 in Figure 2. The amplitude of *Per* oscillations is small because $V_{1max}^{HB3} < V_{1max}^{WT}$. Interestingly, at larger values of V_{3max} and/or α_{PC}, oscillations with a circadian period emerge in Figure 10C, blue symbols. However, the amplitude of *Per* oscillations is again small due to $V_{1max}^{HB3} < V_{1max}^{WT}$.

We remark that the continuation of the bifurcation point HB_4 has similar features as the continuation of HB_3. In Suppl. Fig. S2-S3, we explore interactions between the PC and ROR loops, and the REV and ROR loops, respectively. Taken together, our two-parameter bifurcation diagrams show that interlocked feedback loops generate multiple domains of oscillations in Relogio's model.

The Role of the REV Feedback Loop

In the intertwined dynamics of Relogio model, the REV loop plays a dominant role for tightly balancing positive and negative interactions [16]. To further understand the role of the REV negative-feedback loop, we simplified Relogio's model by approximating some of the state variables as constants, thereby reducing the number of ODEs in the model. For example, when the state variables PC $(x_2 + x_3)$ and x_6 (nuclear protein, ROR_N) are fixed at constant levels, the original model composed of 19 ODE's can be reduced to 7 ODE's describing the state variables in the REV-BMAL loop only (Eqs. (S21-27)). Although such an overly simplified model cannot serve for modeling experimental data, it is helpful for uncovering the role of the REV loop.

For appropriately chosen fixed values of *PC* and x_6, Eqs. (S21-27) display oscillatory dynamics. In Figure 11, we plot a bifurcation diagram on (V_{3max}, V_{5max}), for $x_6^0 = 6$ and $PC^0 = 2.04$. The black curve shows the locus of Hopf bifurcation points in the reduced model. For the sake of comparison, we plot in Figure 11 (dashed green line) the locus of Hopf bifurcation points HB_1 in the full model. The oscillatory domains in the reduced and full models have similar shapes. Moreover, as Suppl. Fig. S4 shows, the REV-BMAL loop can drive circadian oscillations independently of the PC and ROR loops.

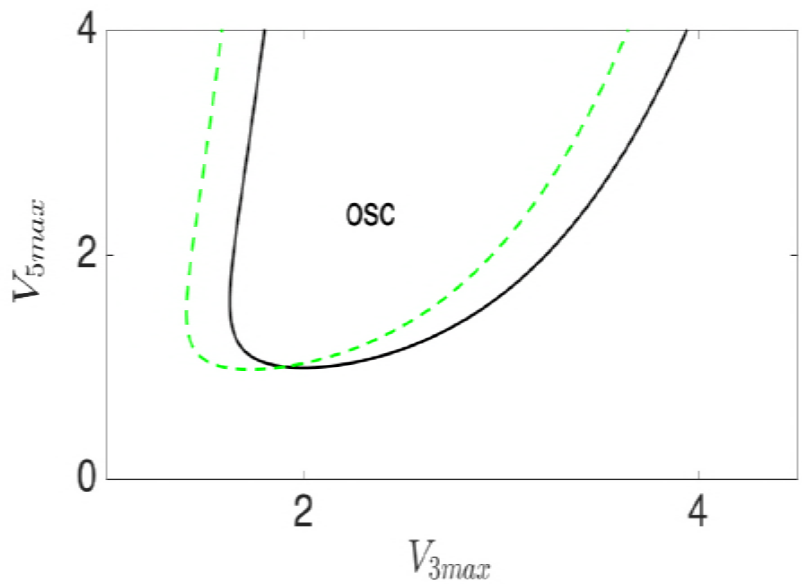

Figure 11. Two-parameter bifurcation diagram on the (V_{3max}, V_{5max}) plane. The solid black curve shows the locus of Hopf bifurcation points in the reduced seven-variable model (Eqs. (S21-27)). The dashed green curve shows the locus of HB_1 (Figure 2) in the full Relogio model. Other parameters of the reduced model are the same as Relogio's WT parameters, and $x_6^0 = 6$ and $PC^0 = 2.04$.

Constitutive expression of REV. The dashed green curve in Figure 12 shows the locus of HB_1 and HB_2 in Figure 2 on the parameter plane (c, V_{5max}). Parameter c is the Hill exponent for *PC*'s repression of *Per* expression in Eq. (S11). Inside the dashed green lines, Relogio's model displays oscillatory dynamics with a circadian period. It was reported in Ref. [16] that when REV is constitutively expressed, the circadian rhythm is lost; for example, when REV_N level is held constant at $x_5^0 = 2.4$. Note that when $x_5(t) = x_5^0 = const$, Relogio's model reduces to a system of 16 ODEs. If the fixed value of x_5^0 is further increased, the reduced model recovers oscillatory dynamics [16].

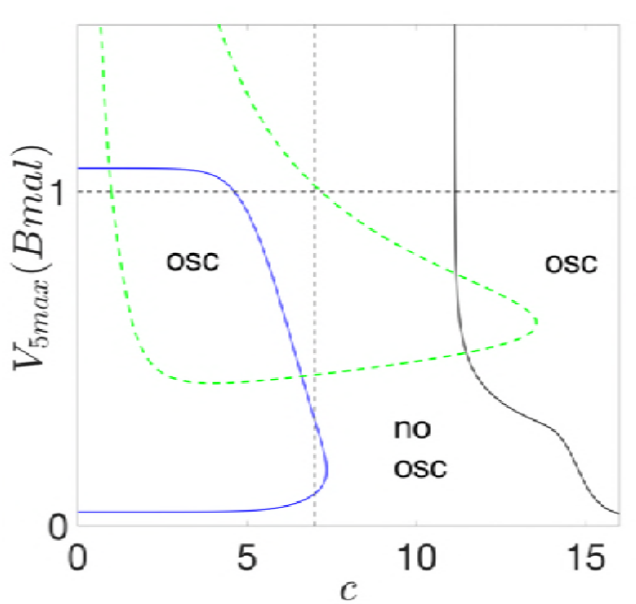

Figure 12. Two-parameter bifurcation diagram. The dashed green curve shows the locus of Hopf bifurcation points HB_1 and HB_2 in Figure 2. If the level of REV is fixed at $x_5^0 = 2.4$, the system becomes non-oscillatory. However, at different values of the parameter c in Eq. S11, two independent oscillatory domains emerge. The blue solid curve bounds a domain of slow oscillations (period > 35 h) at small c. The black curve shows a boundary of oscillations at larger c, where the period of oscillations is ~20 h.

Dashed lines in Figure 12 mark WT values of c and V_{5max}. When $x_5^0 = 2.4$, the reduced model displays a steady-state solution. We found that if the transcription rate of *Bmal* is reduced from its WT value, an oscillatory domain shown by the blue solid line emerges in Figure 12. Here the period (T > 35 h) is larger than the period of circadian oscillations. Because the domain of slow oscillations is persistent at $c = 0$, the role of PC loop can become negligible in this region.

There is yet another oscillatory domain shown by the solid black line in Figure 12, at larger values of c. Because at larger values of c the repression of *PER* gene expression by PC is stronger, the PC loop recovers its intensity in this domain. Here the period of the oscillations is smaller (~20 h) than the period of WT oscillations (~23.5 h). These oscillations persist even if BMAL and ROR loops become constitutive ($x_1^0 = 4.1, x_6^0 = 13$).

The recovery of oscillations dampened by constitutive expression of REV suggests that the balance of positive and negative regulations in the network of interlocked loops is critical for maintaining the circadian rhythm. When REV is constitutively overexpressed ($x_5^0 = 2.4$), the synergy of interlocked loops is lost and the balance of positive and negative regulations is shifted towards the dominance of positive regulation. To recover oscillatory dynamics, either the intensity of the positive feedback needs to be weakened (decreasing V_{5max}) or the intensity of the negative feedback needs to be strengthened (increasing c). Thus, the critical role of the REV loop in

Relogio's model is in interfacing and synergizing positive and negative regulations of the multiple interlocked loops.

Deformation of oscillatory domains. The core-clock network interacts with other pathways in the cell and responds to global regulatory signals in the organism. Depending on how an external signal modulates the core clock network, rhythmic dynamics can be distorted; hence, the underlying oscillatory domains can be deformed. Such dynamic transformations of the core clock network can be studied by bifurcation analysis.

In this subsection, we illustrate deformations of an oscillatory domain in Relogio's model when the REV loop is modulated. We consider two hypothetical modulations, both acting on the variable x_5 (nuclear protein REV_N).

Modulation #1: we assume in Eq. (1) that as a result of external perturbations, the production of nuclear protein REV_N can be increased or decreased by a factor β_{x5},

$$\frac{dx_5}{dt} = \beta_{x5} k_{i,z6} z_6 - d_{x5} x_5. \quad (1)$$

Modulation #2: we assume in Eq. (2) simultaneous perturbation of the rates of production and degradation of REV_N, so that the parameter β_{x5} now modulates the time scale of x_5,

$$\frac{dx_5}{dt} = \beta_{x5}(k_{i,z6} z_6 - d_{x5} x_5). \quad (2)$$

In both cases, the WT value of $\beta_{x5} = 1$.

In the first case, we replaced the ODE for x_5 (Eq. (S6)) in Relogio's model with Eq. (1). Figure 13 shows the two-parameter bifurcation diagram on (V_{1max}, β_{x5}). The green dashed curve shows the locus of Hopf bifurcation points HB_1 and HB_2 in Figure 2; the mauve dashed line shows the locus of Hopf bifurcation points HB_3 and HB_4 in Figure 2. Inside the mauve and green lines, there are two separate oscillatory domains with slow and circadian oscillations, respectively. Both domains shrink and disappear with changing values of β_{x5}.

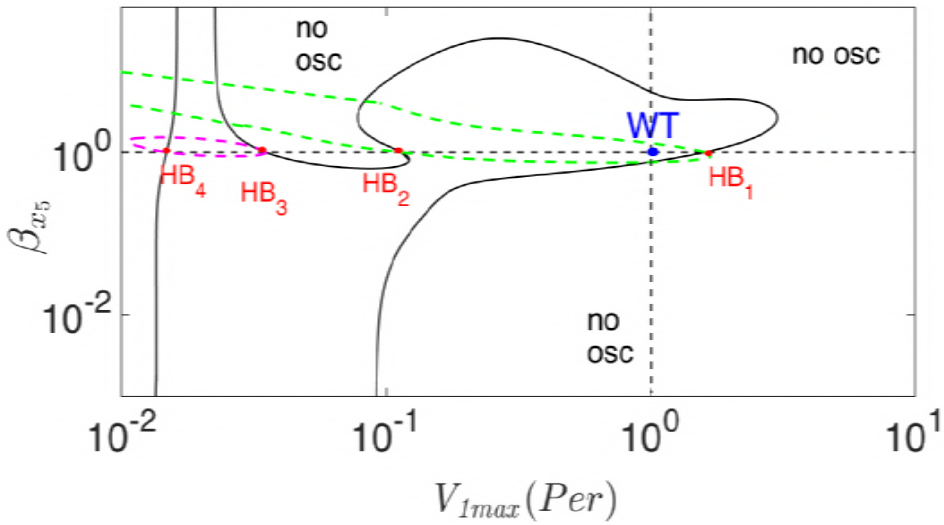

Figure 13. Modulations of the REV feedback loop. β_{x5} is a parameter introduced in Eq. (1) and Eq. (2) to modulate, respectively, either the level of x_5 (nuclear protein REV_N) or the time-scale of x_5. Dashed green and mauve lines are obtained using Eq. (1). $HB_i (i = 1..4)$ mark the Hopf bifurcation points in Figure 2. Solid black lines are obtained using Eq. (2). Inside the solid lines, the system displays oscillatory dynamics.

Next, we replace Eq. (S6) with Eq. (2). The two black, solid curves in Figure 13 show the loci of the Hopf bifurcation points $HB_i, i = 1..4,$ in Figure 2. In contrast to the mauve and green lines, there is a single domain inside the black curves. At small values of β_{x5} and V_{1max}, or at large β_{x5} but small V_{1max}, the black lines are almost parallel to each other. In these regions, there are only two intersections of the oscillatory domain with a horizontal line. Clearly, the domain of oscillation is larger for the solid curves; remarkably, its size increases with an increase of β_{x5}, above the intersections of dashed lines. Note that emergent domains of oscillations are also possible in Figure 13, similar to the slow oscillations shown in Figure 10 by black symbols.

In order to effectively synchronize cellular processes, the core clock network must be resilient to various perturbations. As Figure 13 shows, robustness of the rhythm in the network against parametric modulations can be characterized by deformation of an oscillatory domain. The dashed lines in Figure 13 show that oscillatory domains may shrink if the perturbation modulates the production of REV_N in Eq. (1). But the solid lines in Figure 13 show that if the processes counterbalancing such a perturbation can be activated, as in Eq. (2), the size of a circadian domain can be increased. As enlargement of an oscillatory domain typically implies enhancement of the rhythm's robustness, modulations from other pathways in the cell may strengthen the synergy of the feedback loops. Interestingly, the interactions between core clock and cell cycle networks is interfaced by the REV loop [24, 29] which plays a critical role in the synergy of the interlocked loop.

Discussions

Comprehensive mathematical models of fundamental biological processes, such as circadian rhythms or cell cycle controls, play important roles in molecular systems biology. Bifurcation analysis is a powerful tool for qualitative characterization of these mathematical models [21, 36]. For a model with many variables and parameters, bifurcation analysis can be very informative and also very challenging. In this paper, we have used bifurcation analysis to decipher the roles of interlocked feedback loops in a model of the mammalian circadian-clock network, namely, a model proposed by Relogio et al. [16].

Current understanding of the mammalian circadian-clock network is incomplete. Bioinformatics studies revealed more than 40 genes that directly interact with the core clock genes [37]. Together, known clock genes form an extended core clock network [37]. A detailed mathematical model of the extended network has not been developed yet, but obviously it will include many new variables and parameters. The parameters whose modulations cause qualitative changes in network dynamics uncover susceptible components and feedback loops. The one- and two-parameter bifurcation diagrams presented in this work illustrate the dynamic changes of period, amplitude and phase of oscillations, as well as deformations of oscillatory domains in the core clock network, in dependence on parametric modulations. These modulations represent processes controlling gene expression, protein stability, feedback intensities, etc. The effects of the genes in the extended network on the core clock dynamics can be assessed from the bifurcation diagrams presented in this work.

Depending on how an oscillatory model is built and parameterized, the mechanisms generating oscillations can be different. Unlike previous models of circadian oscillations, which rely chiefly on the classical Goodwin-type mechanism of oscillation [12], i.e., a single negative-feedback transcription-translation loop, the circadian rhythm in Relogio's model is driven by two synergetic feedback loops, PC and RBR. Our bifurcation analysis shows that (similar to the Goodwin mechanism) the PC loop can display a single Hopf bifurcation point as the vertical line in Figure 9 shows. In Figure 9, the persistence of oscillations with the increase of *Cry*'s transcription rate is consistent with the *Cry*-overexpression phenotype retaining circadian rhythmicity. On the other hand, a bifurcation diagram of the RBR loop typically displays a second Hopf bifurcation point as the horizontal line in Figure 8 shows, due to the positive feedback exerted on *REV*. Such behavior is consistent with the reported aperiodic dynamics for gene overexpression in the RBR loop [16]. Thus, the interlocking mechanism explains overexpression phenotypes in mice, by combining contrasting dynamics: *Cry* overexpression retains rhythmicity, gene overexpression in the RBR loop loses rhythmicity [16].

In Relogio's model, the RBR loop plays a special role. Oscillations persist if the PC loop is non-oscillatory ($x_2 = const, x_3 = const$), but they damp out if the RBR loop is non-oscillatory. It was reported that when *REV* is constitutively expressed ($x_5^0 = 2.4$), WT oscillations are damped out [16]. However, we find that, even with constitutively overexpressed *REV* ($x_5^0 = 2.4$) oscillations are possible at different values of the parameter c (see Figure 12). These oscillations are generated by the PC and RBR loops independently in two separate domains. In the first domain, oscillations are slow and persistent even if the PC loop is constitutive. In the second domain, oscillations are

rapid and persistent even if the BMAL and ROR loops are constitutive. Thus, it is the REV loop that enables the synergy of positive and negative feedback loops to generate robust circadian rhythms in Relogio's model.

In extended models, the circadian core clock network is integrated to other pathways in the cell, which can themselves display autonomous oscillation [24, 25, 29, 32, 35]. A plethora of oscillatory mechanisms and domains of oscillations are possible in such models. Intuitively, the size, shape, and number of oscillatory domains can be indicators of robustness of rhythmic dynamics. But how the interplay of different oscillatory mechanisms is regulated and how complex networks integrate oscillatory domains are still unknown and remain major goals of future studies [13].

Acknowledgements

Financial Assistance from the Department of Biological Sciences and the College of Science at Virginia Tech is gratefully acknowledged. DB was partially supported by a grant from the Mongolian Foundation for Science and Technology. The authors thank Dr. S. Kojima for fruitful discussions. DB is thankful to Dr. Angela Relogio for explaining the results published in [16].

Author Contributions

Designed research (DB) and (JJT); performed research (DB); visualization (DB); wrote the manuscript (DB) and (JJT).

References

1. Reppert SM, Weaver DR. Coordination of circadian timing in mammals. Nature. 2002;418(6901):935-41. Epub 2002/08/29. doi: 10.1038/nature00965. PubMed PMID: 12198538.
2. Roden LC, Carré IA. The molecular genetics of circadian rhythms in Arabidopsis. Semin Cell Dev Biol. 2001;12(4):305-15. doi: 10.1006/scdb.2001.0258. PubMed PMID: 11463215.
3. Xue Z, Ye Q, Anson SR, Yang J, Xiao G, Kowbel D, et al. Transcriptional interference by antisense RNA is required for circadian clock function. Nature. 2014;514(7524):650-3. Epub 2014/08/19. doi: 10.1038/nature13671. PubMed PMID: 25132551; PubMed Central PMCID: PMCPMC4214883.
4. Mori T, Johnson CH. Circadian programming in cyanobacteria. Semin Cell Dev Biol. 2001;12(4):271-8. Epub 2001/07/21. doi: 10.1006/scdb.2001.0254. PubMed PMID: 11463211.
5. Loros JJ, Dunlap JC. Genetic and molecular analysis of circadian rhythms in Neurospora. Annual review of physiology. 2001;63:757-94. Epub 2001/02/22. doi: 10.1146/annurev.physiol.63.1.757. PubMed PMID: 11181975.
6. Goldbeter A. Biochemical Oscillations and Cellular Rhythms: The Molecular Bases of Periodic and Chaotic Behaviour: Cambridge University Press; 1997.
7. Kurosawa G, Aihara K, Iwasa Y. A model for the circadian rhythm of cyanobacteria that maintains oscillation without gene expression. Biophys J. 2006;91(6):2015-23. Epub 2006/06/27. doi: 10.1529/biophysj.105.076554. PubMed PMID: 16798799; PubMed Central PMCID: PMCPMC1557573.
8. Goodwin BC. Oscillatory behavior in enzymatic control processes. Advances in enzyme regulation. 1965;3:425-38. Epub 1965/01/01. PubMed PMID: 5861813.
9. Gonze D, Abou-Jaoude W. The Goodwin model: behind the Hill function. PloS one. 2013;8(8):e69573. Epub 2013/08/13. doi: 10.1371/journal.pone.0069573. PubMed PMID: 23936338; PubMed Central PMCID: PMCPMC3731313.
10. Tyson JJ, Othmer HG. The dynamics of feedback control circuits in biochemical pathways. Prog Theor Biol. 1978;5:1-62.
11. Kim JK, Forger DB. A mechanism for robust circadian timekeeping via stoichiometric balance. Molecular systems biology. 2012;8:630. Epub 2012/12/06. doi: 10.1038/msb.2012.62. PubMed PMID: 23212247; PubMed Central PMCID: PMCPMC3542529.
12. Mirsky HP, Liu AC, Welsh DK, Kay SA, Doyle FJ. A model of the cell-autonomous mammalian circadian clock. Proceedings of the National Academy of Sciences. 2009;106(27):11107-12. doi: 10.1073/pnas.0904837106.
13. Leloup J-C, Goldbeter A. Toward a detailed computational model for the mammalian circadian clock. Proceedings of the National Academy of Sciences of the United States of America. 2003;100(12):7051-6. doi: 10.1073/pnas.1132112100. PubMed PMID: PMC165828.
14. Korenčič A, Bordyugov G, Košir R, Rozman D, Goličnik M, Herzel H. The Interplay of cis-Regulatory Elements Rules Circadian Rhythms in Mouse Liver. PloS one. 2012;7(11):e46835. doi: 10.1371/journal.pone.0046835. PubMed PMID: PMC3489864.
15. Hong CI, Jolma IW, Loros JJ, Dunlap JC, Ruoff P. Simulating Dark Expressions and Interactions of frq and wc-1 in the Neurospora Circadian Clock. Biophysical Journal. 2008;94(4):1221-32. doi: 10.1529/biophysj.107.115154.
16. Relógio A, Westermark PO, Wallach T, Schellenberg K, Kramer A, Herzel H. Tuning the Mammalian Circadian Clock: Robust Synergy of Two Loops. PLOS Computational Biology. 2011;7(12):e1002309. doi: 10.1371/journal.pcbi.1002309.

17. Yan J, Shi G, Zhang Z, Wu X, Liu Z, Xing L, et al. An intensity ratio of interlocking loops determines circadian period length. Nucleic Acids Research. 2014;42(16):10278-87. doi: 10.1093/nar/gku701.
18. Saithong T, Painter KJ, Millar AJ. The Contributions of Interlocking Loops and Extensive Nonlinearity to the Properties of Circadian Clock Models. PloS one. 2010;5(11):e13867. doi: 10.1371/journal.pone.0013867.
19. Pett JP, Korenčič A, Wesener F, Kramer A, Herzel H. Feedback Loops of the Mammalian Circadian Clock Constitute Repressilator. PLoS Computational Biology. 2016;12(12):e1005266. doi: 10.1371/journal.pcbi.1005266. PubMed PMID: PMC5189953.
20. Foo M, Somers DE, Kim P-J. Kernel Architecture of the Genetic Circuitry of the Arabidopsis Circadian System. PLOS Computational Biology. 2016;12(2):e1004748. doi: 10.1371/journal.pcbi.1004748.
21. Battogtokh D, Tyson JJ. Bifurcation analysis of a model of the budding yeast cell cycle. Chaos (Woodbury, NY). 2004;14(3):653-61. Epub 2004/09/28. doi: 10.1063/1.1780011. PubMed PMID: 15446975.
22. Anafi RC, Lee Y, Sato TK, Venkataraman A, Ramanathan C, Kavakli IH, et al. Machine Learning Helps Identify CHRONO as a Circadian Clock Component. PLoS Biology. 2014;12(4):e1001840. doi: 10.1371/journal.pbio.1001840. PubMed PMID: PMC3988006.
23. Hong CI, Zámborszky J, Baek M, Labiscsak L, Ju K, Lee H, et al. Circadian rhythms synchronize mitosis in Neurospora crassa. Proceedings of the National Academy of Sciences. 2014;111(4):1397-402. doi: 10.1073/pnas.1319399111.
24. Gerard C, Goldbeter A. Entrainment of the mammalian cell cycle by the circadian clock: modeling two coupled cellular rhythms. PLoS Comput Biol. 2012;8(5):e1002516. Epub 2012/06/14. doi: 10.1371/journal.pcbi.1002516. PubMed PMID: 22693436; PubMed Central PMCID: PMCPMC3364934.
25. Tyson JJ, Novák B. Functional Motifs in Biochemical Reaction Networks. Annual Review of Physical Chemistry. 2010;61(1):219-40. doi: 10.1146/annurev.physchem.012809.103457. PubMed PMID: 20055671.
26. Hartwell LH, Hopfield JJ, Leibler S, Murray AW. From molecular to modular cell biology. Nature. 1999.
27. Traynard P, Feillet C, Soliman S, Delaunay F, Fages F. Model-based investigation of the circadian clock and cell cycle coupling in mouse embryonic fibroblasts: Prediction of RevErb-alpha up-regulation during mitosis. Bio Systems. 2016;149:59-69. Epub 2016/07/23. doi: 10.1016/j.biosystems.2016.07.003. PubMed PMID: 27443484.
28. Bieler J, Cannavo R, Gustafson K, Gobet C, Gatfield D, Naef F. Robust synchronization of coupled circadian and cell cycle oscillators in single mammalian cells. Molecular systems biology. 2014;10:739. Epub 2014/07/17. doi: 10.15252/msb.20145218. PubMed PMID: 25028488; PubMed Central PMCID: PMCPMC4299496.
29. Gérard C, Goldbeter A. Temporal self-organization of the cyclin/Cdk network driving the mammalian cell cycle. Proceedings of the National Academy of Sciences of the United States of America. 2009;106(51):21643-8. doi: 10.1073/pnas.0903827106. PubMed PMID: PMC2799800.
30. Battogtokh D, Aihara K, Tyson JJ. Synchronization of eukaryotic cells by periodic forcing. Physical review letters. 2006;96(14):148102. Epub 2006/05/23. doi: 10.1103/PhysRevLett.96.148102. PubMed PMID: 16712125.
31. Kornmann B, Schaad O, Bujard H, Takahashi JS, Schibler U. System-Driven and Oscillator-Dependent Circadian Transcription in Mice with a Conditionally Active Liver Clock. PLOS Biology. 2007;5(2):e34. doi: 10.1371/journal.pbio.0050034.
32. Battogtokh D, Kojima S, Tyson JJ. Modeling the interactions of sense and antisense Period transcripts in the mammalian circadian clock network. PLoS Comput Biol. 2018;14(2):e1005957. Epub 2018/02/16. doi: 10.1371/journal.pcbi.1005957. PubMed PMID: 29447160.

33. Doedel E, Champneys A, Dercole F, Fairgrieve T, Kuznetsov Y, Oldeman B, et al. Auto: {S}oftware for continuation and bifurcation problems in ordinary differential equations. 2009.
34. Relogio A, Thomas P, Medina-Perez P, Reischl S, Bervoets S, Gloc E, et al. Ras-mediated deregulation of the circadian clock in cancer. PLoS genetics. 2014;10(5):e1004338. Epub 2014/05/31. doi: 10.1371/journal.pgen.1004338. PubMed PMID: 24875049; PubMed Central PMCID: PMCPMC4038477.
35. El-Athman R, Genov NN, Mazuch J, Zhang K, Yu Y, Fuhr L, et al. The Ink4a/Arf locus operates as a regulator of the circadian clock modulating RAS activity. PLOS Biology. 2017;15(12):e2002940. doi: 10.1371/journal.pbio.2002940.
36. Borisuk MT, Tyson JJ. Bifurcation analysis of a model of mitotic control in frog eggs. Journal of theoretical biology. 1998;195(1):69-85. Epub 1998/11/06. doi: 10.1006/jtbi.1998.0781. PubMed PMID: 9802951.
37. Lehmann R, Childs L, Thomas P, Abreu M, Fuhr L, Herzel H, et al. Assembly of a comprehensive regulatory network for the mammalian circadian clock: a bioinformatics approach. PloS one. 2015;10(5):e0126283. Epub 2015/05/07. doi: 10.1371/journal.pone.0126283. PubMed PMID: 25945798; PubMed Central PMCID: PMCPMC4422523.

Supplementary Material

Supplementary Text S1: Differential equations of the Relogio et al. model.

http://journals.plos.org/ploscompbiol/article?id=10.1371/journal.pcbi.1002309

CLOCK/BMAL

$$\frac{dx1}{dt} = kf_{x1}x7 - kd_{x1}x1 - d_{x1}x1 \tag{S1}$$

Rev-Erb

$$\frac{dy3}{dt} = V_{3\max}\frac{1+g\left(\frac{x1}{k_{t3}}\right)^{v}}{1+\left(\frac{PC}{k_{i3}}\right)^{w}\left(\frac{x1}{k_{t3}}\right)^{v}+\left(\frac{x1}{k_{t3}}\right)^{v}} - d_{y3}y3 \tag{S2}$$

Ror

$$\frac{dy4}{dt} = V_{4\max}\frac{1+h\left(\frac{x1}{k_{t4}}\right)^{p}}{1+\left(\frac{PC}{k_{i4}}\right)^{q}\left(\frac{x1}{k_{t4}}\right)^{p}+\left(\frac{x1}{k_{t4}}\right)^{p}} - d_{y4}y4 \tag{S3}$$

REV-ERB$_C$

$$\frac{dz6}{dt} = k_{p3}(y3+y3_0) - ki_{z6}z6 - d_{z6}z6 \tag{S4}$$

ROR$_C$

$$\frac{dz7}{dt} = k_{p4}(y4+y4_0) - ki_{z7}z7 - d_{z7}z7 \tag{S5}$$

REV-ERB$_N$

$$\frac{dx5}{dt} = ki_{z6}z6 - d_{x5}x5 \tag{S6}$$

ROR$_N$

$$\frac{dx6}{dt} = ki_{z7}z7 - d_{x6}x6 \tag{S7}$$

Bmal

$$\frac{dy5}{dt} = V_{5\max}\frac{1+i\left(\frac{x6}{k_{t5}}\right)^n}{1+\left(\frac{x5}{k_{i5}}\right)^m+\left(\frac{x6}{k_{t5}}\right)^n} - d_{y5}y5 \tag{S8}$$

BMAL$_C$

$$\frac{dz8}{dt} = k_{p5}(y5+y5_0) - ki_{z8}z8 - d_{z8}z8 \tag{S9}$$

BMAL$_N$

$$\frac{dx7}{dt} = ki_{z8}z8 + kd_{x1}x1 - kf_{x1}x7 - d_{x7}x7 \tag{S10}$$

Per

$$\frac{dy1}{dt} = V_{1\max}\frac{1+a\left(\frac{x1}{k_{t1}}\right)^b}{1+\left(\frac{PC}{k_{i1}}\right)^c\left(\frac{x1}{k_{t1}}\right)^b+\left(\frac{x1}{k_{t1}}\right)^b} - d_{y1}y1 \tag{S11}$$

Cry

$$\frac{dy2}{dt} = V_{2\max} \frac{1 + d\left(\frac{x1}{k_{t2}}\right)^{e}}{1 + \left(\frac{PC}{k_{i2}}\right)^{f}\left(\frac{x1}{k_{t2}}\right)^{e} + \left(\frac{x1}{k_{t2}}\right)^{e}} \frac{1}{1 + \left(\frac{x5}{k_{i21}}\right)^{f1}} - d_{y2}y2 \tag{S12}$$

CRY_C

$$\frac{dz1}{dt} = k_{p2}(y2 + y2_0) + kd_{z4}z4 + kd_{z5}z5 - kf_{z5}z1z2 - kf_{z4}z1z3 - d_{z1}z1 \tag{S13}$$

PER_C

$$\frac{dz2}{dt} = k_{p1}(y1 + y1_0) + kd_{z5}z5 + kd_{phz3}z3 - kf_{z5}z2z1 - kph_{z2}z2 - d_{z2}z2 \tag{S14}$$

PER_C^*

$$\frac{dz3}{dt} = kph_{z2}z2 + kd_{z4}z4 - kd_{phz3}z3 - kf_{z4}z3z1 - d_{z3}z3 \tag{S15}$$

PER_C^*/CRY_C

$$\frac{dz4}{dt} = kf_{z4}z1z3 + ke_{x2}x2 - ki_{z4}z4 - kd_{z4}z4 - d_{z4}z4 \tag{S16}$$

PER_C/CRY_C

$$\frac{dz5}{dt} = kf_{z5}z1z2 + ke_{x3}x3 - ki_{z5}z5 - kd_{z5}z5 - d_{z5}z5 \tag{S17}$$

PER^*_N/CRY_N

$$\frac{dx2}{dt} = ki_{z4}z4 - ke_{x2}x2 - d_{x2}x2 \tag{S18}$$

PER_N/CRY_N

$$\frac{dx3}{dt} = ki_{z5}z5 - ke_{x3}x3 - d_{x3}x3 \tag{S19}$$

PER/CRY_{pool}

$$PC = x2 + x3 \tag{S20}$$

Seven-variable Model of BMAL-REV loops ($x_6 = x_6^0 = 6$ and $PC = PC^0 = 2.04$)

CLOCK/BMAL

$$\frac{dx1}{dt} = kf_{x1}x7 - kd_{x1}x1 - d_{x1}x1 \tag{S21}$$

Rev-Erb

$$\frac{dy3}{dt} = V_{3\max}\frac{1+g\left(\frac{x1}{k_{t3}}\right)^v}{1+\left(\frac{PC}{k_{i3}}\right)^w\left(\frac{x1}{k_{t3}}\right)^v+\left(\frac{x1}{k_{t3}}\right)^v} - d_{y3}y3 \tag{S22}$$

REV-ERB$_C$

$$\frac{dz6}{dt} = k_{p3}(y3+y3_0) - ki_{z6}z6 - d_{z6}z6 \tag{S23}$$

REV-ERB$_N$

$$\frac{dx5}{dt} = ki_{z6}z6 - d_{x5}x5 \tag{S24}$$

Bmal

$$\frac{dy5}{dt} = V_{5\max}\frac{1+i\left(\frac{x6}{k_{t5}}\right)^n}{1+\left(\frac{x5}{k_{i5}}\right)^m+\left(\frac{x6}{k_{t5}}\right)^n} - d_{y5}y5 \tag{S25}$$

BMAL$_C$

$$\frac{dz8}{dt} = k_{p5}(y5+y5_0) - ki_{z8}z8 - d_{z8}z8 \tag{S26}$$

BMAL$_N$

$$\frac{dx7}{dt} = ki_{z8}z8 + kd_{x1}x1 - kf_{x1}x7 - d_{x7}x7 \tag{S27}$$

Suppl. Table S1. Variables in the Relogio et al Model

Variable	Name
x1	CLOCK/BMAL
x2	PER^{*}_{N}/CRY_{N}
x3	PER_{N}/CRY_{N}
PC	PER/CRY_{pool}
x5	$REV\text{-}ERB_{N}$
x6	ROR_{N}
y1	*Per*
y2	*Cry*
y3	*Rev-Erb*
y4	*Ror*
y5	*Bmal*
z1	CRY_{C}
z2	PER_{C}
z3	PER_{C}^{*}
z4	PER_{C}^{*}/CRY_{C}
z5	PER_{C}/CRY_{C}
z6	$REV\text{-}ERB_{C}$
z7	ROR_{C}
z8	$BMAL_{C}$

Suppl. Table S2. Wild Type Parameter Values

Parameter	Name	Value
Degradation rates for nuclear proteins or nuclear protein complexes [hour^{-1}]		
d_{x1}	CLOCK/BMAL	0.08
d_{x2}	PER^{*}_{N}/CRY_{N}	0.06
d_{x3}	PER_{N}/CRY_{N}	0.09
d_{x5}	$REV\text{-}ERB_{N}$	0.17
d_{x6}	ROR_{N}	0.12
d_{x7}	$BMAL_{N}$	0.15
Degradation rates for mRNAs [hour^{-1}]		
d_{y1}	*Per*	0.3
d_{y2}	*Cry*	0.2
d_{y3}	*Rev-Erb*	2
d_{y4}	*Ror*	0.2
d_{y5}	*Bmal*	1.6
Degradation rates for cytoplasmic proteins [hour^{-1}]		
d_{z1}	CRY_{C}	0.23
d_{z2}	PER_{C}	0.25
d_{z3}	PER_{C}^{*}	0.6
d_{z4}	PER_{C}^{*}/CRY_{C}	0.2
d_{z5}	PER_{C}/CRY_{C}	0.2
d_{z6}	$REV\text{-}ERB_{C}$	0.31
d_{z7}	ROR_{C}	0.3
d_{z8}	$BMAL_{C}$	0.73
Reaction rates for complex formation/dissociation		
kf_{x1}	CLOCK/BMAL-complex formation **[hour^{-1}]**	2.3
kd_{x1}	CLOCK/BMAL-complex dissociation **[hour^{-1}]**	0.01
kf_{z4}	PER_{C}^{*}/CRY_{C}-complex formation **[(a.u.·hour)$^{-1}$]**	1
kd_{z4}	PER_{C}^{*}/CRY_{C}-complex dissociation **[hour^{-1}]**	1
kf_{z5}	PER_{C}/CRY_{C}-complex formation **[(a.u.·hour)$^{-1}$]**	1
kd_{z5}	PER_{C}/CRY_{C}-complex dissociation **[hour^{-1}]**	1

Phosphorylation/dephosphorylation reaction rates [hour^{-1}]		
kph_{z2}	PER_C-phosphorylation rate	2
kd_{phz3}	PER_C^{*-}dephosphorylation rate	0.05
Transcription rates [a.u.·hour^{-1}]		
V_{1max}	*Per*	1
V_{2max}	*Cry*	2.92
V_{3max}	*Rev-Erb*	1.9
V_{4max}	*Ror*	10.9
V_{5max}	*Bmal*	1
Activation/inhibition rates [a.u.]		
k_{t1}	*Per*-activation rate	3
k_{i1}	*Per*-inhibition rate	0.9
k_{t2}	*Cry*-activation rate	2.4
k_{i2}	*Cry*-inhibition rate	0.7
k_{i21}	*Cry*-inhibition rate	5.2
k_{t3}	*Rev-Erb*-activation rate	2.07
k_{i3}	*Rev-Erb*-inhibition rate	3.3
k_{t4}	*Ror*-activation rate	0.9
k_{i4}	*Ror*-inhibition rate	0.4
k_{t5}	*Bmal*-activation rate	8.35
k_{i5}	*Bmal*-inhibition rate	1.94
Transcription fold activation (dimensionless)		
a	*Per*	12
d	*Cry*	12
g	*Rev-Erb*	5
h	*Ror*	5
i	*Bmal*	12
Production rates [hour^{-1}]		
k_{p1}	PER_C	0.4
k_{p2}	CRY_C	0.26
k_{p3}	$REV\text{-}ERB_C$	0.37
k_{p4}	ROR_C	0.76
k_{p5}	$BMAL_C$	1.21

	Import/Export rates [hour^{-1}]	
ki_{z4}	PER_C^*/CRY_C	0.2
ki_{z5}	PER_C/CRY_C	0.1
ki_{z6}	$REV\text{-}ERB_C$	0.5
ki_{z7}	ROR_C	0.1
ki_{z8}	$BMAL_C$	0.1
ke_{x2}	PER^*_N/CRY_N	0.02
ke_{x3}	PER_N/CRY_N	0.02
	Hill exponents of transcription (dimensionless)	
b	*Per*-activation	5
c	*Per*-inhibition	7
e	*Cry*-activation rate	6
f	*Cry*-inhibition	4
f1	*Cry*-inhibition	1
v	*Rev-Erb*-activation	6
w	*Rev-Erb*-inhibition	2
p	*Ror*-activation	6
q	*Ror*-inhibition	3
n	*Bmal*-activation	2
m	*Bmal*-inhibition	5
	Exogenous RNA [a.u.]	
$y1_0$	*Per*	0
$y2_0$	*Cry*	0
$y3_0$	*Rev-Erb*	0
$y4_0$	*Ror*	0
$y5_0$	*Bmal*	0

Supplementary Figures

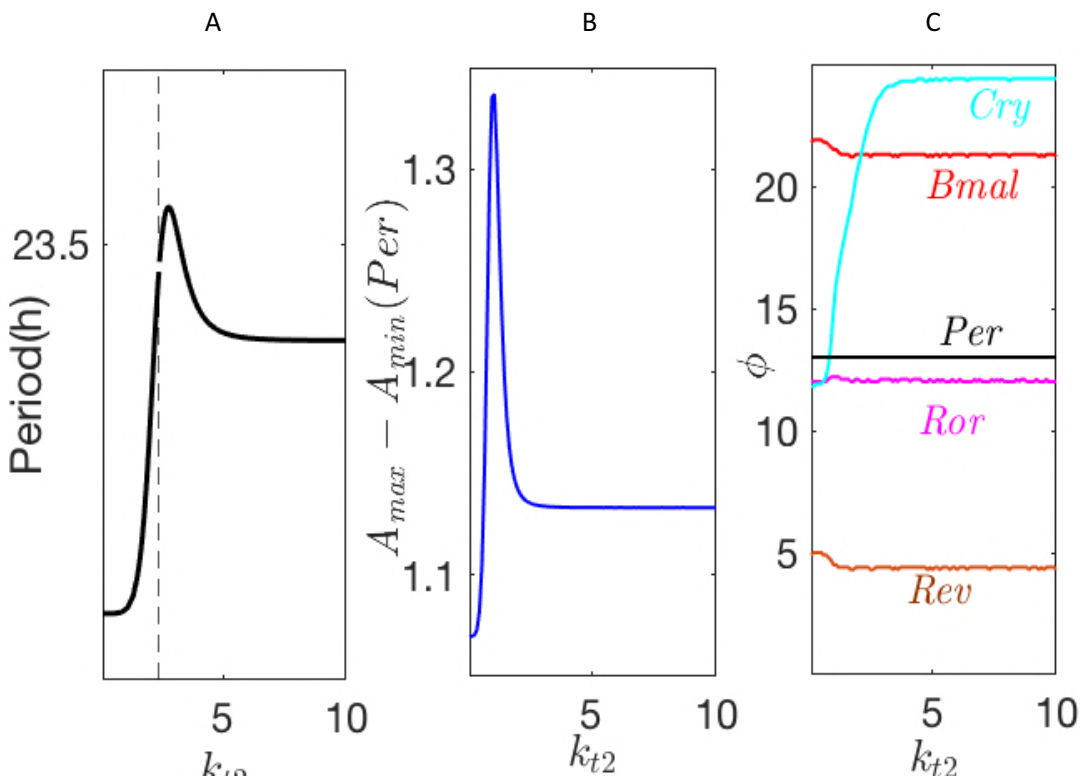

Fig. S1. The effects of RAS signaling on the circadian clock network. Parameter k_{t2} (Eq. (S12)) is used as the bifurcation parameter. A) Period. B) Maximum amplitude of *Per*. C) Phases of oscillations. The vertical dashed line in A marks the WT value of k_{t2}.

Two-parameter bifurcation diagrams characterizing the ROR loop

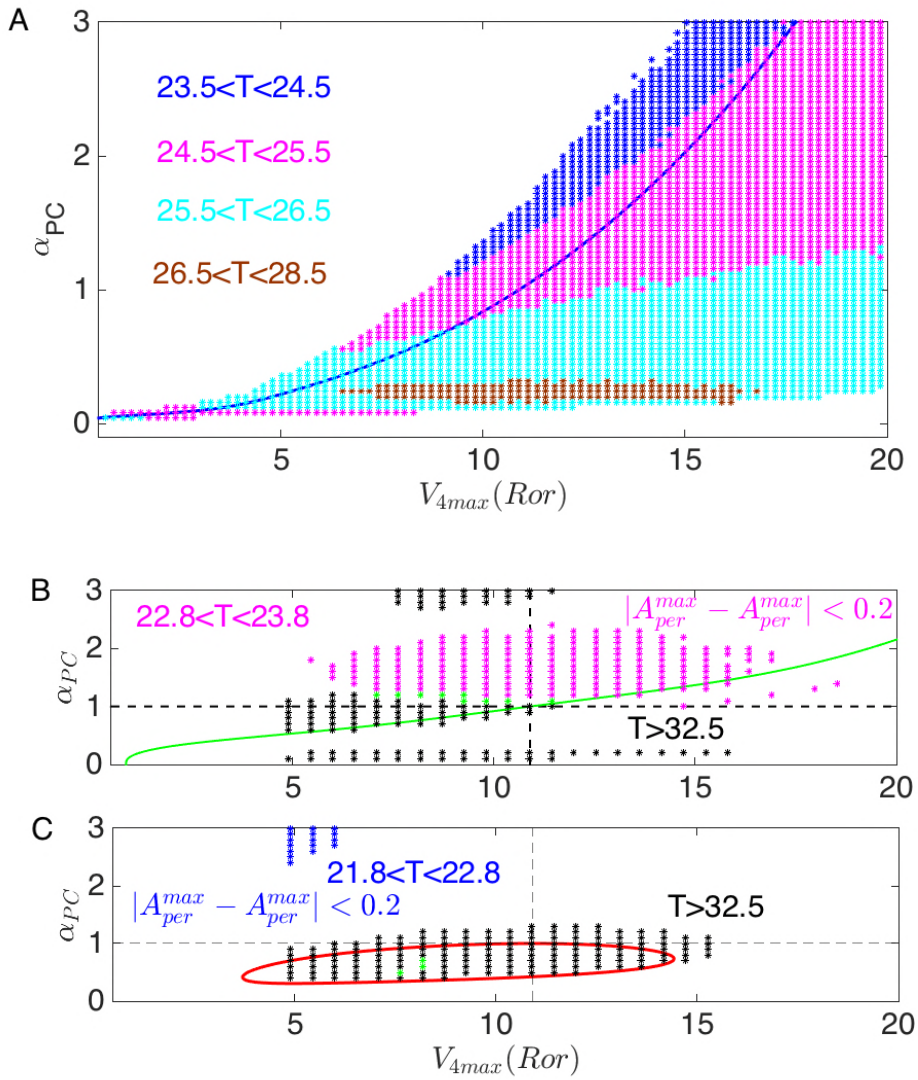

Fig. S2. Interactions between PC and ROR loops. (A) The blue line shows the continuation of Hopf bifurcation point HB_1 in Figure 2. Symbols in different colors mark oscillation periods for $V_{1max} = 1$. (B) The green line marks the continuation of Hopf bifurcation point HB_2 in Figure 2. Symbols of purple and black colors mark oscillation periods for $V_{1max} = 0.1$. Dashed lines mark WT values of the bifurcation parameters. (C) The red curve marks the continuation of Hopf bifurcation point HB_3 in Figure 2. Symbols of blue and black colors mark oscillation periods for $V_{1max} = 0.05$. Green symbols show that besides the domain of slow oscillations, there is a tiny region of circadian oscillations inside the loci of HB_3.

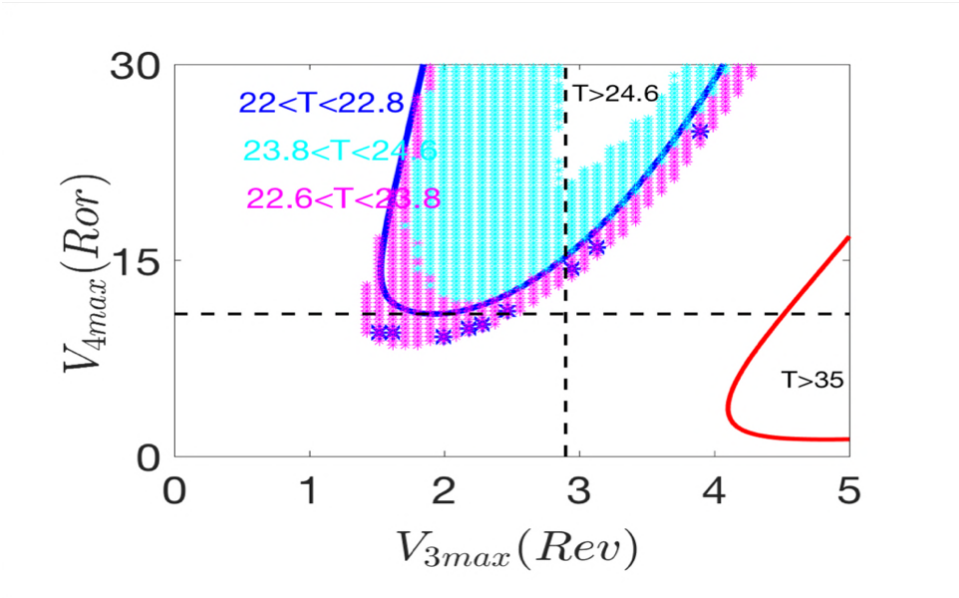

Fig. S3. A two-parameter bifurcation diagram on (V_{3max}, V_{4max}). The blue curve shows the continuation of the Hopf bifurcation point HB_1 in Figure 2. Symbols of different colors mark oscillation periods for $V_{1max} = 1.60$. Dashed lines mark WT values of the bifurcation parameters. The red curve indicates a domain of emergent slow oscillations.

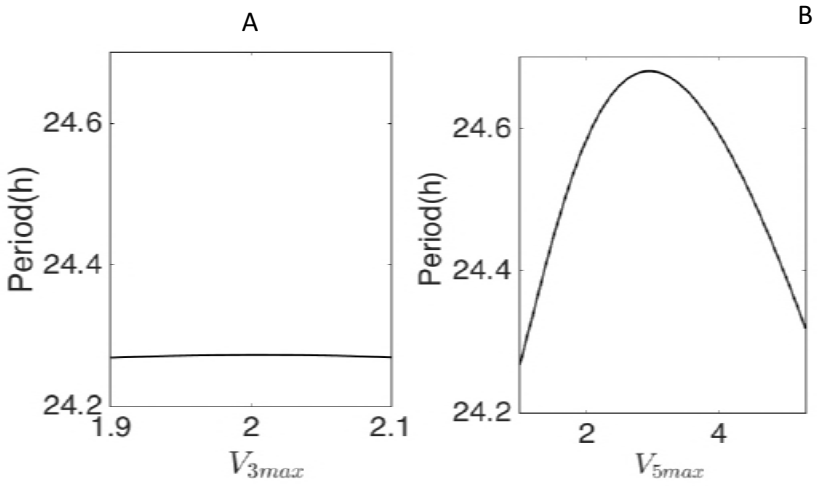

Fig. S4. Period of oscillations vs transcription rates in the reduced seven-ODE model (Eq. (S1-S7)). Left: Period vs V_{3max}. Right: Period vs V_{5max}.